Inorganic Chemistry

Article

pubs.acs.org/IC

Structural Evolution under Pressure of $BiMnO_3$

Gianluca Calestani,*[,†] Fabio Orlandi,[†] Francesco Mezzadri,[†] Lara Righi,[†,‡] Marco Merlini,[§] and Edmondo Gilioli[‡]

[†]Dipartimento di Chimica, Università degli Studi di Parma, Parco Area delle Scienze 17A, I-43124 Parma, Italy

[‡]CNR-IMEM, Parco Area delle Scienze 37A, I-43124 Parma, Italy

[§]Dipartimento di Scienze della Terra, Università degli Studi di Milano, Via Botticelli 23, I-20133 Milano, Italy

Supporting Information

ABSTRACT: The structural behavior of $BiMnO_3$ under pressure was studied in a quantitative way by single-crystal synchrotron X-ray diffraction up to 36 GPa. Two phase transitions were observed at moderate pressures (1 and 6 GPa, respectively), leading the system at first to the $P2_1/c$ and then to the *Pnma* symmetry. The breaking of *C*-centering in the first transition does not affect significantly Jahn−Teller (JT) distortion and orbital order (OO) but determines a significant change in the cooperative tilting of the MnO_6 octahedra. The second transition increases the symmetry to orthorhombic, leading to a *Pnma* structure similar to the O′ structure of $LaMnO_3$, characterized by $a > c > b/\sqrt{2}$. No symmetry change was observed above 7.1 GPa, but the different compressibility of the lattice parameters (in particular, the *b* axis) leads at first to a pseudocubic phase (≈30 GPa) and then to different parameter ratios ($b/\sqrt{2} > c > a$). Even if the JT distortion is continuously reduced with increasing pressure, it is retained, together with the resulting OO, until the highest measured pressure, pointing out the relevant role of the distortion induced by the Bi^{3+} lone pair in stabilizing the JT distortion.

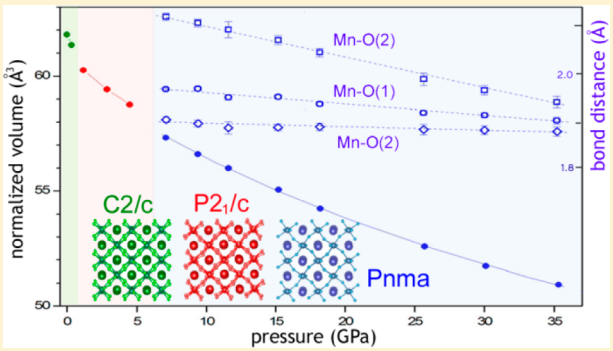

INTRODUCTION

Magnetoelectric multiferroic materials,[1] combining electric and magnetic order, attract attention in solid-state physics, also in view of possible applications in new electronic devices.[2−6] Among the various magnetoelectrics reported in recent years, $BiMnO_3$, synthesized under high pressure,[7,8] is a rare example of ferromagnetic (FM) material. The FM ordering, observed at T_c = 100 K in this system,[9] originates by superexchange[10,11] taking place in the presence of a peculiar orbital ordering (OO) resulting from a heavily distorted perovskite structure. Compared to $LaMnO_3$, which has an antiferromagnetic (AFM) ground state also originating from OO and superexchange,[12,13] the FM state in $BiMnO_3$ is at first sight surprising and points out the relevance of the distortion induced by the Bi^{3+} $6s^2$ lone pair in determining the peculiar OO pattern. In recent years, both the structure and the properties of $BiMnO_3$ have been a matter of debate, some doubt being expressed as to whether it is multiferroic at all. It has been generally accepted that the $BiMnO_3$ phase I, metastable at room temperature (RT) and ambient pressure (AP), crystallizes in the noncentrosymmetric space group *C*2.[14,15] However, a centrosymmetric *C*2/*c* structure, incompatible with ferroelectricity (FE), was later suggested by first-principles calculations[16] and confirmed by experimental studies[17,18] performed not only at RT but also below the magnetic transition. More recently, Solovyev and Pchelkina[19−21] put forward the idea that FE in $BiMnO_3$ could be improper, being related to the competition between the FM state (with *C*2/*c* symmetry, deriving from conventional nearest-neighbor interactions) and a hidden ↑↓↓↑ AFM state, which breaks the inversion symmetry (produced by the peculiar OO via longer-range interactions between remote Mn atoms). The idea that the structure could be rather instable and could be easily modified by small variations of external parameters, suggested by the competition of FM and AFM states, found further support in the complex structural behavior of $BiMnO_3$. A minority polymorph with a higher magnetic T_C (107 K) was found to coexist at RT with phase I in the as-prepared material and to disappear on heating,[22] where two reversible transitions were observed at 470 and 770 K.[14,23] The first one leads to a further monoclinic phase (II), whose structure was determined in *C*2/*c* by Belik el al.,[17] whereas the latter to a $LaMnO_3$-related orthorhombic phase (III). The structure of $BiMnO_3$ is known also to depend on its oxygen stoichiometry.[24,25] By increasing the Mn^{4+} content (produced by cation deficiency) indeed, the symmetry evolves again to orthorhombic *Pnma* through two different monoclinic modifications (*C*2/*c* and $P2_1/c$, respectively), each one characterized by peculiar magnetic properties and decreasing T_C. A similar structural trend was observed by increasing the pressure[26,27] up to 10 GPa: a new monoclinic phase was found to be stable above 1 GPa and to convert to the orthorhombic *Pnma* one in the 6−8 GPa range. The symmetry

Received: June 18, 2014
Published: July 31, 2014

   dx.doi.org/10.1021/ic5013878 | *Inorg. Chem.* 2014, 53, 8749−8754

Table 1. Crystal Data for the $BiMnO_3$ Structure at Different Pressures

P (GPa)	phase	system	s.g.	a (Å)	b (Å)	c (Å)	β (deg)	V (Å^3)	D_x (g/cm^3)
0.35	I	monocl.	$C2/c$	9.513(3)	5.5941(5)	9.836(11)	110.37(8)	490.7(2)	8.44
1.2	P	monocl.	$P2_1/c$	9.6230(13)	5.46038(19)	9.824(4)	110.96(3)	482.05(8)	8.59
2.9	P	monocl.	$P2_1/c$	9.5921(5)	5.43141(8)	9.7664(19)	110.872(14)	475.42(7)	8.71
4.5	P	monocl.	$P2_1/c$	9.5619(6)	5.40751(9)	9.725(2)	110.795(14)	470.07(8)	8.81
7.1	O′	orthorh.	$Pnma$	5.5282(3)	7.5899(9)	5.4641(11)	90	229.26(8)	9.03
9.4	O′	orthorh.	$Pnma$	5.4987(2)	7.5692(7)	5.4400(8)	90	226.42(7)	9.15
11.6	O′	orthorh.	$Pnma$	5.4708(6)	7.5494(15)	5.4221(19)	90	223.94(9)	9.25
15.2	O′	orthorh.	$Pnma$	5.4294(6)	7.5233(14)	5.3913(18)	90	220.22(10)	9.40
18.2	O′	orthorh.	$Pnma$	5.3910(5)	7.4997(14)	5.3650(18)	90	216.91(9)	9.58
25.7	O′	orthorh.	$Pnma$	5.3104(7)	7.4649(18)	5.306(2)	90	210.32(11)	9.85
30.1	O′	orthorh.	$Pnma$	5.2708(4)	7.4467(10)	5.2725(12)	90	206.94(8)	10.01
35.3	O′	orthorh.	$Pnma$	5.2235(4)	7.4274(12)	5.241(12)	90	203.72(7)	10.19

of the intermediate monoclinic phase was determined as $P2_1/c$ by a synchrotron X-ray powder diffraction experiment,[26] whereas, in a further neutron diffraction study, the structure was refined in $C2/c$.[27] It is interesting to note that the high-pressure orthorhombic phase was reported to present an OO similar to that of $LaMnO_3$, which is regarded as the archetypal cooperative Jahn−Teller (JT) and orbitally ordered system. Generally speaking, the JT distortion is expected to be reduced under pressure (potentially until a total suppression), but the details of this evolution as well as the occurrence of an eventual total suppression have been debated.[28−30] In fact, it was first claimed, by synchrotron X-ray diffraction, that the JT was completely suppressed in $LaMnO_3$ above 18 GPa,[28] before further measurements by Raman and X-ray absorption spectroscopy suggested a persistence of the JT distortion, coexisting with a new emergent undistorted phase, up to 34 GPa well above the insulator-to-metal transition.[29,30] The discrepancy with X-ray results suggests that the phase segregation revealed by these techniques occurs on a spatial or time scale that cannot be accessed by X-ray diffraction. Since Bi^{3+} has an ionic radius very similar to that of La^{3+} but a stereochemistry that is strongly influenced by its $6s^2$ lone-pair character, the comparison of the structural behavior of $LaMnO_3$ and $BiMnO_3$ under high pressure is considered quite important in order to understand the possible role of the lone-pair-induced distortion in stabilizing JT distortion and OO. Very recently, two different studies appeared in the literature,[31,32] dealing with structural characterization of $BiMnO_3$ at pressures above 10 GPa. In the first one,[31] beside a P−T phase diagram obtained by means of energy-dispersive powder X-ray diffraction in the ranges of 0−4 GPa and 300−900 K, the structural behavior at high pressures and ambient temperature of $BiMnO_3$ was studied by means of angle-dispersive powder XRD and Raman spectroscopy up to 50 GPa. At $P > 20$ GPa, a structural phase transition from *Pnma* to a new orthorhombic *Imma* phase was reported. Following the authors, the transition would start at $P \sim 20$ GPa, evolving over a pressure range of several GPa, leading to the suppression of the long-range $d(3_{y^2-r^2})$ e_g OO, being the static cooperative JT distortion forbidden in *Imma*. Completely different results were obtained by synchrotron XRD and Raman spectroscopy up to 60 GPa.[32] The *Pnma* structure was found to remain remarkably stable between 7 and 37 GPa, and no transition to *Imma* was observed. On the contrary, the transition to a strongly elongated monoclinic phase was found to occur between 37 and 39 GPa, followed by the transition to a triclinic metallic phase above 53 GPa. On the basis of the Rietveld refinement of the powder XRD data collected at 50 GPa, the authors claim that the high-pressure monoclinic structure is noncentrosymmetric and allows ferroelectricity, which contradicts the traditional expectation that ferroelectricity vanishes under pressure. However, given the history of the determination of the structure of phase I of $BiMnO_3$, any assignment of noncentrosymmetry, on the basis of powder XRD, should be prudent, especially given the quality of the data available at such high pressures. In the same work, the structural study under pressure was also attempted by using "single" crystals, but the observed twinning made a full structural refinement impossible in the whole pressure range. Concurrently, we performed a similar synchrotron XRD experiment. Unfortunately, our study was limited in pressure to 36 GPa so that a more limited pressure range was explored. However, the data were collected from single crystals that demonstrated to be suitable for similar experiments, offering us the possibility to accurately reinvestigate, in a quantitative way, the structural behavior of $BiMnO_3$ under pressure, in order to clarify aspects that remained controversial after previous investigations.

EXPERIMENTAL SECTION

Diffraction experiments were performed at the ID9A beamline of the ESRF (Grenoble)[33] by monochromatic X-ray radiation (λ = 0.41456 Å). Wavelength and geometrical instrumental parameters (sample-to-detector distance, beam center, detector tilt) were refined against standard silicon powder and a pure quartz single crystal. $BiMnO_3$ single crystals were extracted from a ceramic sample and prepared by high-pressure−high-temperature synthesis (4 GPa, 1073 K) from a mixture of the binary oxides containing a slight Bi_2O_3 excess. The crystal quality of small fragments, with dimensions ranging around a few microns, were preliminarily tested on the beamline. A small crystal with dimensions of 5 × 5 × 4 μm^3, practically free from the usual twinning arising in $BiMnO_3$ by the phase transitions occurring at the end of the preparation process by the final temperature decrease and pressure release, was selected and mounted in a diamond anvil cell (DAC), used for pressure generation with helium as a pressure medium to provide nearly hydrostatic conditions. Diffraction data suitable for structure solution and refinement were collected at 293 K with a Mar555 flat panel detector in the range of $2.5 < \theta < 19°$ by 0.5° ω step in the angular interval of ±30° for 12 pressure steps ranging from 0.35 to 35.3 GPa. The intensity integration was performed with the Oxford Diffraction software CrysalisRed-171.32.29 (Oxford Diffraction Ltd., Abingdon, England), using the profile fitting algorithm and no model refinement. Empirical rescaling and absorption correction were applied. The structures were solved by direct methods with SIR2004[34] and refined with anisotropic atomic displacements parameters (a.d.p.) for Bi and Mn atoms by using JANA2006[35] for all the investigated pressures.

dx.doi.org/10.1021/ic5013878 | Inorg. Chem. 2014, 53, 8749−8754

RESULTS

Crystal data for all the investigated pressures are reported in Table 1. Refinement parameters, atomic coordinates, and Mn−O bond distances are reported as Supporting Information in Tables SI and SII, respectively, for four selected examples that are representative of the observed behavior. As expected by previous investigations,[26,27,31,32] two phase transitions are clearly observed around 1.0 and 6.0 GPa, respectively. However, differently from what was reported for powder samples, the transitions are quite sharp and no coexistence of different phases was observed in our single-crystal experiments. This suggests that the wide phase coexistence previously observed in powder experiments is not intrinsic but likely originates from stress between grains or local inhomogeneities, which, in turn, underlines the importance of the single-crystal experiments we performed.

The first transition, keeping the monoclinic symmetry, breaks the *C*-centering typical of phase I. The $P2_1/c$ space group was assigned to the new phase (hereinafter indicated as P) on the basis of systematic absences. This result agrees with previously published synchrotron data[26,31] and indicates that the use of $C2/c$ symmetry to refine the structure by neutron data[27] was probably dictated by insufficient resolution or poor data quality. The second transition (P = 6.0 GPa) increases the symmetry to orthorhombic, leading to a *Pnma* structure similar to the O′ structure of $LaMnO_3$,[36−38] characterized by $a > c > b/\sqrt{2}$. According to Table 1, no symmetry change was observed above 7.1 GPa, but the different compressibility of the lattice parameters (in particular, of the b axis) leads at first to a pseudocubic phase (≈30 GPa) and then to different parameter ratios ($b/\sqrt{2} > c > a$). This is shown in Figure 1, where the

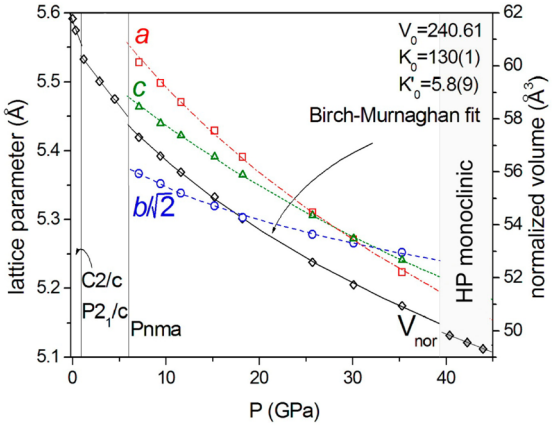

Figure 1. Pressure dependence of (right axis) $BiMnO_3$ cell volume, normalized to the fundamental perovskite lattice to compare different phases (the values of the HP monoclinic phase are taken from ref 32) and (left axis) lattice parameters of the orthorhombic cell occurring at higher pressure; *b*-axis data are normalized by a factor of $(1/\sqrt{2})$, corresponding to a pseudocubic lattice representation.

pressure dependence of the lattice parameters of the orthorhombic structure and the behavior of the cell volume (normalized to the fundamental perovskite lattice in order to compare different phases) is reported. It was found that the $V(P)$ data of the orthorhombic structure are well described by the Birch−Murnaghan equation[39] and the derived bulk modulus K_0 and its pressure derivative K'_0 at zero pressure are reported in Figure 1. It is interesting to note that an orthorhombic *Pnma* modification has been observed under pressure in similar conditions (above 10 GPa) also in $BiFeO_3$,[40] but in this case, the cell parameters reveal an almost linear pressure-dependent evolution. The analysis of the Mn−O bond distances at the 1.0 GPa transition indicates that the breaking of *C*-centering does not affect significantly the JT distortion. The OO scheme of phase P is similar to that of phase I and is shown schematically in Figure 2. On the contrary, the phase transition

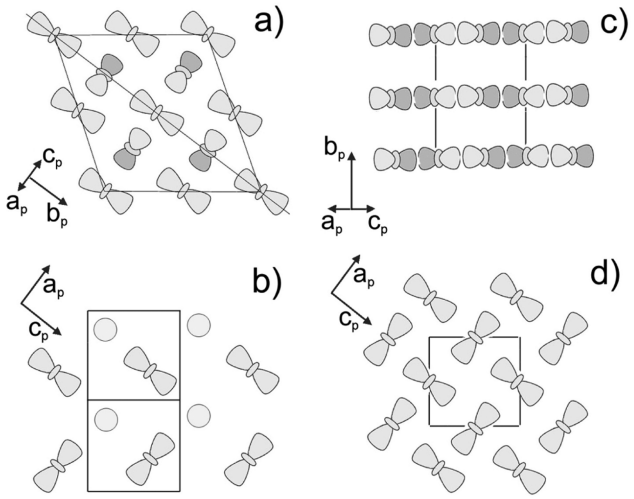

Figure 2. Orbital ordering in $BiMnO_3$ structures: (a, b) monoclinic phases (I and P); (c, d) orthorhombic *Pnma* phase. Only the occupied e_g orbitals of Mn^{3+} are shown; a_p, b_p, and c_p refer to the fundamental perovskite axes.

determines a significant change in the cooperative tilting of the MnO_6 octahedra. As shown in Figure 3, the in-plane tilt in adjacent perovskite layers, which propagates with an opposite phase in I, becomes in-phase in P so that the final transition to O′ simply involves the equivalence of the adjacent layers by the increased symmetry.

As shown in Figure 4, the structural rearrangement involved into the I−P transition results in a significant change of the Mn−O−Mn angles, which become dispersed over a wider range. The Mn−O−Mn angles tend to decrease by increasing pressure, before the sudden collapse in the 148−150° range at the P−O′ transition. The structure of O′-$BiMnO_3$ is similar to that of $LaMnO_3$, even if an important shift of the O(2) atom position is produced in $BiMnO_3$ by the necessity to accommodate the Bi^{3+} $6s^2$ lone pair.

The strong JT distortion observed in the monoclinic phases survives in O′, but the pattern of the occupied e_g orbitals changes drastically and, in analogy with $LaMnO_3$, develops parallel to the *ac* plane, as shown in Figure 2. Being the two compounds characterized by similar OO and space symmetry, the same magnetic behavior of $LaMnO_3$, i.e., A-type AFM, is, in principle, expected for orthorhombic $BiMnO_3$. The pressure evolution of the O′ structure is resumed in Figure 5. The linear decrease of the Mn−O distances, observed with increasing pressure, suggests a progressive reduction of the cooperative JT effect, a process that could be completed at about 45 GPa, if the observed trends would be maintained beyond the maximum applied pressure: in this case, at this pressure, all the bond lengths are expected to become nearly equivalent by extrapolation of the observed trends. It is interesting to note that this pressure is much higher than the one required for the observation of OO quenching in $LaMnO_3$ by XRD (18 GPa),

dx.doi.org/10.1021/ic5013878 | Inorg. Chem. 2014, 53, 8749−8754

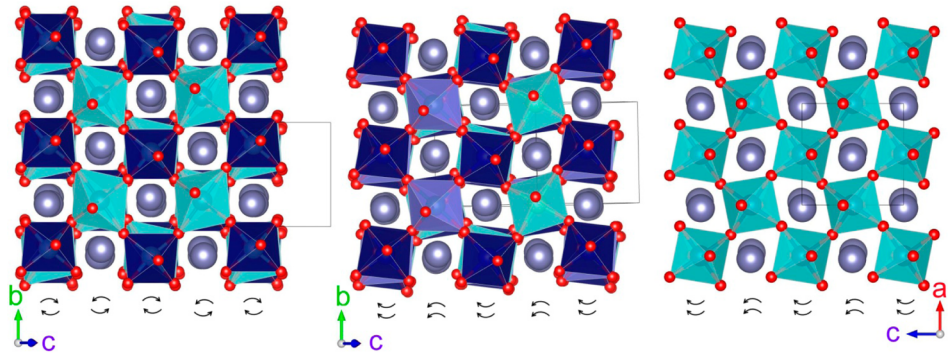

Figure 3. Pressure-dependent evolution of the $BiMnO_3$ structure (from left to right: phase I, P, and O′), projected along the same fundamental perovskite axis (determined by the analysis of the orientation matrices). Arrows show schematically the in-plane tilt of MnO_6 octahedra in layers alternating along the view axis. Different colors refer to symmetry-independent octahedra.

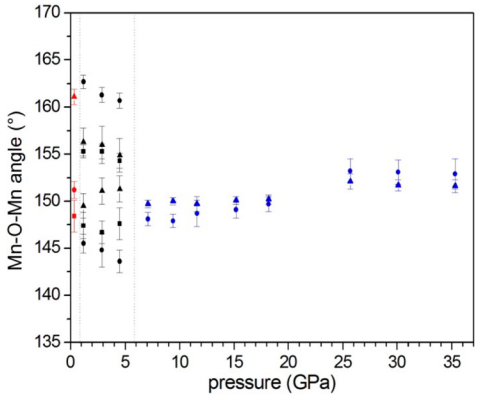

Figure 4. Pressure dependence of the Mn−O−Mn angles. In red, black, and blue are reported the data corresponding to the $C2/c$, $P2_1/c$, and *Pnma* phases, respectively.

pointing out the relevant role of the Bi^{3+} lone pair in stabilizing the JT distortion of trivalent manganese. Quite interesting is also the behavior of the Mn−O−Mn angles, which increase under pressure in the orthorhombic phase, at least until the pseudocubic minimization of the lattice parameter distortion is reached. The increase is more evident for the angle involving the apical O(1) atom, and this is probably driven by the decrease of the apical Mn−O(1) distance. The two Mn−O−Mn angles are frozen above 25 GPa, and the structural stress cumulated in this region could be at the origin of the further transition observed above 37 GPa. Our structure analysis shows that the distortion of the Bi environment, originated by the steric requirements of the lone-pair accommodation, persists in the whole range analyzed in spite of the increase of the number of shorter Bi−O interactions (<2.65 Å) observed with increasing pressure (Figure 6). Moreover, calculations performed on the basis of the lattice parameters derived by the Birch−Murnaghan fit and of the atomic coordinates extrapolated by the observed trends show that the stereoactive effect of the Bi^{3+} $6s^2$ lone pair would be still present at 45 GPa, pressure for which the JT distortion is expected to vanish if the transition above 37 GPa would not be observed; in these conditions, the 12 Bi−O distances would still vary over a wide range, three distances being close to 2.20 Å, five ranging from 2.45 to 2.60 Å, one reaching 2.8 Å, and the longest three lying beyond 3.0 Å.

By analyzing the interplay between orbital ordering and lattice distortions in $LaMnO_3$, Mizokawa et al.[41] found that a

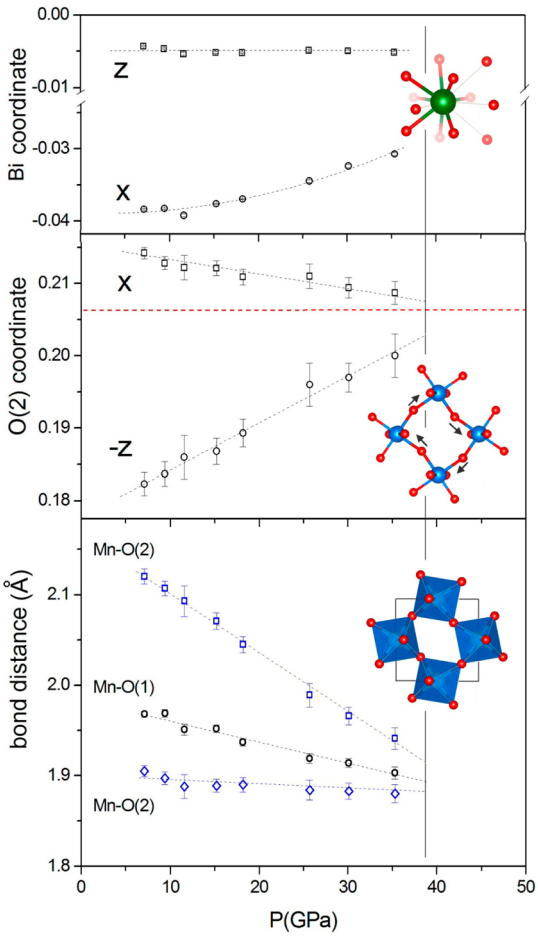

Figure 5. Pressure dependence of Mn−O distances and selected coordinates in the O′ phase. Structural insets show (from top to bottom): the distorted coordination of Bi at 35 GPa showing the eight Bi−O interactions shorter than 2.6 Å; effects of the O(2) coordinates shift; the almost regular coordination of Mn at 35 GPa (just before the transition to monoclinic).

relatively large $GdFeO_3$-type structural distortion is essential to stabilize the orbital ordering, lowering the energy of the d-type JT distortion that is responsible for the A-type AFM ground state. It is quite interesting to note that, in $LaMnO_3$, the shift of the La ion along the x coordinate, at the basis of the $GdFeO_3$-type distortion, decreases progressively with increasing pressure,[28] vanishing just before the destabilization of OO at

dx.doi.org/10.1021/ic5013878 | Inorg. Chem. 2014, 53, 8749−8754

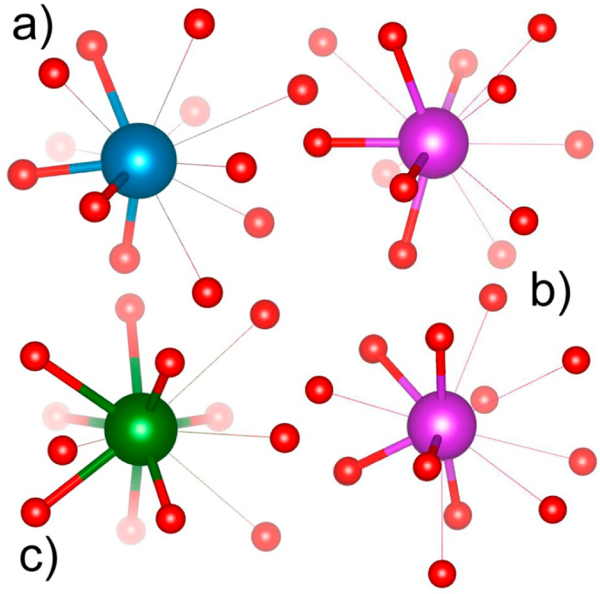

Figure 6. Pressure-induced evolution of the asymmetric dodecahedral oxygen environments of the Bi atom in the I (a, blue), P (b, purple), and O′ (c, green) structures. The shorter bonds (<2.65 Å) are depicted as cylinders, while the longer ones are indicated by thin lines. Despite the increase of the number of shorter Bi−O interactions observed with increasing pressure, the asymmetric lone-pair character of the Bi atom is retained.

high pressures. Consequently, the quenching of OO seems to be directly driven by the progressive reduction of this distortion. This does not occur in the case of $BiMnO_3$, where the x shift is involved also in the accommodation of the stereochemical requirements of the Bi atom. As shown in Figure 5, the x shift, even if slightly reduced, persists to the highest pressure, and a different structural mechanism, allowing the destabilization of OO, must be necessarily taken into account. The mechanism consists of a shift of the O(2) coordinates in the ac plane, where the x and $-z$ values of O(2) tend to converge with increasing pressure.

The extrapolation (Figure 5) shows that the $x = -z$ condition, corresponding to the coalescence of the two independent Mn−O(2) distances at ≈1.89 Å, would occur again. This is in agreement with the hypothesis of a quenching of OO at 45 GPa, in the absence of the further phase transition.

DISCUSSION AND CONCLUSIONS

By comparing the obtained results with literature data, it is quite interesting to note that any variation of external (T, P) or internal (composition) parameters leading to a potential vanishing of JT distortion and OO induces in $BiMnO_3$ structural variations that develop in an analogous manner. Similar intermediate monoclinic phases are produced, and the process ends up in an orthorhombic phase strictly related to $LaMnO_3$. For example, the disordered presence of Mn^{4+} in the lattice, produced in both $LaMnO_3$ and $BiMnO_3$ by oxygen nonstoichiometry, leads the two phases to a pseudocubic *Pnma* structure, in which the OO is completely suppressed; moreover, almost identical lattice parameters are observed for a Mn^{4+} content of about 25%[25,42] in the two compounds. A similar behavior is observed by increasing the temperature; as shown by resonant X-ray scattering,[43] the OO melting occurs in $BiMnO_3$ at T = 770 K, in conjunction with the monoclinic−orthorhombic transition involving phases II and III. Noteworthy is the fact that also $BiMnO_3$-III has lattice parameters[23] similar to the pseudocubic ones observed for $LaMnO_3$ at 780 K,[36] just above its OO melting, occurring at 750 K. On the basis of these results, the lone-pair character of Bi^{3+}, which is responsible for the peculiar OO in $BiMnO_3$ and, consequently, for its unusual properties, seems, therefore, to lose importance at high temperature or in the presence of the structural disorder perturbing the OO, as the one induced by the increase of the oxidation state of manganese. In these conditions, the compound tends to behave like $LaMnO_3$, in particular, once OO has vanished. However, under pressure, the situation changes completely and the persisting distortion induced by the lone-pair character of Bi^{3+} seems to play an important role in stabilizing JT and OO. In order to understand this phenomenon, we need to consider that the usual strategy adopted by the asymmetric lone-pair Bi^{3+} ion to be hosted in high symmetry structures involves the setting of a statistically disordered off-centering. This is certainly favored by a lattice expansion, for example, by increasing temperature, but is prevented at high pressure where, because of the volume shrinking, the lone-pair distortion cannot be apparently symmetrized and its vanishing would require a change of the electronic configuration. Our structural results show that, thanks to the persistence of the lone-pair distortion to the highest pressure in $BiMnO_3$, the OO survives not only to the monoclinic−orthorhombic transition but also, in this latter phase, well beyond the stability limit observed in $LaMnO_3$. Comparison with the data obtained by Guennou et al. at higher pressure[32] shows that, before the JT distortion could collapse in the *Pnma* structure, a further transition to a new, highly distorted, monoclinic phase occurs between 37 and 39 GPa, before the final insulator−metal transition at 53 GPa. A detailed structure analysis of this monoclinic phase would be necessary for a better comprehension of the phenomenon.

ASSOCIATED CONTENT

Supporting Information

The crystallographic information files (CIF) of the I, P, and two O′ $BiMnO_3$ phases, together with complete refinement parameters and selected bond lengths. This material is available free of charge via the Internet at http://pubs.acs.org.

AUTHOR INFORMATION

Corresponding Author

*E-mail: gianluca.calestani@unipr.it.

Author Contributions

All authors have given approval to the final version of the manuscript.

Notes

The authors declare no competing financial interests.

ACKNOWLEDGMENTS

F.O. thanks Fondazione Cariparma for financial support. ESRF is acknowledged for provision of beamtime, and M. Hanfland is acknowledged for assistance at the ID09A beamline.

REFERENCES

(1) Eerenstein, W.; Mathur, N. D.; Scott, J. F. *Nature* **2006**, *442*, 759−765.
(2) Cheong, S.-W.; Mostovoy, M. *Nat. Mater.* **2007**, *6*, 13−20.

(3) Hur, N.; Park, S.; Sharms, P. A.; Ahn, J. S.; Guha, S.; Cheong, S.-W. *Nature* **2004**, *429*, 392−395.
(4) Nan, C.-W.; Bichurin, M. I.; Dong, S.; Viehland, D.; Srinivasan, G. *J. Appl. Phys.* **2008**, *103*, 031101.
(5) Gajek, M.; Bibes, M.; Fusil, S.; Bouzehouane, K.; Fontcuberta, J.; Barthelemy, A.; Fert, A. *Nat. Mater.* **2007**, *6*, 296−302.
(6) Binek, C.; Doudin, B. *J. Phys.: Condens. Matter* **2005**, *17*, L39−L44.
(7) Sugawara, F.; Iida, S.; Syono, Y.; Akimoto, S. *J. Phys. Soc. Jpn.* **1965**, *20*, 1529−1529.
(8) Sugawara, F.; Iida, S.; Syono, Y.; Akimoto, S. *J. Phys. Soc. Jpn.* **1968**, *25*, 1553−1558.
(9) Chiba, H.; Atou, T.; Syono, Y. J. *Solid State Chem.* **1997**, *132*, 139−143.
(10) Atou, T.; Chiba, H.; Ohoyama, K.; Yamaguchi, Y.; Syono, Y. *J. Solid State Chem.* **1999**, *145*, 639−642.
(11) Moreira dos Santos, A.; Cheetham, A. K.; Atou, T.; Syono, Y.; Yamaguchi, Y.; Ohoyama, K.; Chiba, H.; Rao, C. N. R. *Phys. Rev. B* **2002**, *66*, 064425.
(12) Hill, N. A.; Rabe, K. M. *Phys. Rev. B* **1999**, *59*, 8759.
(13) Gonchar', L. E.; Nikiforov, A. E. *Phys. Solid State* **2000**, *42*, 1070−1074.
(14) Kimura, T.; Kawamoto, S.; Yamada, I.; Azuma, M.; Takano, M.; Tokura, Y. *Phys. Rev. B* **2003**, *67*, 180401(R).
(15) Chi, Z. H.; Xiao, C. J.; Feng, S. M.; Li, F. Y.; Jin, C. Q.; Wang, X. H.; Chen, R. Z.; Li, L. Y. *J. Appl. Phys.* **2005**, *98*, 103519.
(16) Baettig, P.; Seshadri, R.; Spaldin, N. A. *J. Am. Chem. Soc.* **2007**, *129*, 9854−9855.
(17) Belik, A. A.; Iikubo, S.; Yokosawa, T.; Kodama, K.; Igawa, M.; Shamoto, S.; Azuma, M.; Takano, M.; Kimoto, K.; Matsui, Y.; Takayama-Muromachi, E. *J. Am. Chem. Soc.* **2007**, *129*, 971−977.
(18) Montanari, E.; Calestani, G.; Righi, L.; Gilioli, E.; Bolzoni, F.; Knight, K. S.; Radaelli, P. G. *Phys. Rev. B* **2007**, *75*, 220101(R).
(19) Solovyev, I. V.; Pchelkina, Z. V. *New J. Phys.* **2008**, *10*, 073021.
(20) Solovyev, I. V.; Pchelkina, Z. V. *Pis'ma Zh. Eksp. Teor. Fiz.* **2009**, *89*, 701; *JETP Lett.* **2009**, *89*, 597.
(21) Solovyev, I. V.; Pchelkina, Z. V. *Phys. Rev. B* **2010**, *82*, 094425.
(22) Montanari, E.; Righi, L.; Calestani, G.; Migliori, A.; Gilioli, E.; Bolzoni, F. *Chem. Mater.* **2005**, *17*, 1765−1773.
(23) Montanari, E.; Calestani, G.; Migliori, A.; Dapiaggi, M.; Bolzoni, F.; Cabassi, R.; Gilioli, E. *Chem. Mater.* **2005**, *17*, 6457−6467.
(24) Sundaresan, A.; Mangalam, R. V. K.; Iyo, A.; Tanaka, Y.; Rao, C. N. R. *J. Mater. Chem.* **2008**, *18*, 2191−2193.
(25) Belik, A. A.; Kolodiazhnyi, T.; Kosuda, K.; Takayama-Muromachi, E. *J. Mater. Chem.* **2009**, *19*, 1593−1600.
(26) Belik, A. A.; Yusa, H.; Hirao, N.; Ohishi, Y.; Takayama-Muromachi, E. *Inorg. Chem.* **2009**, *48*, 1000−1004.
(27) Kozlenko, D. P.; Belik, A. A.; Kichanov, S. E.; Mirebeau, I.; Sheptyakov, D. V.; Strässle, Th.; Makarova, O. L.; Belushkin, A. V.; Savenko, B. N.; Takayama-Muromachi, E. *Phys. Rev. B* **2010**, *82*, 014401.
(28) Loa, I.; Adler, P.; Grzechnik, A.; Syassen, K.; Schwarz, U.; Hanfland, M.; Rozenberg, G. Kh.; Gorodetsky, P.; Pasternak, M. P. *Phys. Rev. Lett.* **2001**, *87*, 125501.
(29) Baldini, M.; Struzhkin, V. V.; Goncharov, A. F.; Postorino, P.; Mao, W. L. *Phys. Rev. Lett.* **2011**, *106*, 066402.
(30) Ramos, A. Y.; Souza-Neto, N. M.; Tolentino, H. C. N.; Bunau, O.; Joly, Y.; Grenier, S.; Itié, J.-P.; Flank, A.-M.; Lagarde, P.; Caneiro, A. *Europhys. Lett.* **2011**, *96*, 36002.
(31) Kozlenko, D. P.; Dang, N. T.; Jabarov, S. H.; Belik, A. A.; Kichanov, S. E.; Lukin, E. V.; Lathe, C.; Dubrovinsky, L. S.; Kazimirov, V. Yu.; Smirnov, M. B.; Savenko, B. N.; Mammadov, A. I.; Takayama-Muromachi, E.; Khiem, L. H. *J. Alloys Compd.* **2014**, *585*, 741−747.
(32) Guennou, M.; Bouvier, P.; Toulemonde, P.; Darie, C.; Goujon, C.; Bordet, P.; Hanfland, M.; Kreisel, J. *Phys. Rev. Lett.* **2014**, *112*, 075501.
(33) Merlini, M.; Hanfland, M. *High Pressure Res.* **2013**, *33*, 511−522.
(34) Burla, M. C.; Caliandro, R.; Camalli, M.; Carrozzini, B.; Cascarano, G. L.; De Caro, L.; Giacovazzo, C.; Polidori, G.; Spagna, R. *J. Appl. Crystallogr.* **2005**, *38*, 381−388.
(35) Petricek, V.; Dusek, M.; Palatinus, L. *Jana2006: The Crystallographic Computing System*; Institute of Physics: Praha, Czech Repub, 2006.
(36) Sakai, L.; Fjellvåg, H.; Lebech, B. *Acta Chem. Scand.* **1997**, *51*, 904−909.
(37) Ritter, C.; Ibarra, M. R.; De Teresa, J. M.; Algarabel, P. A.; Marquina, C.; Blasco, J.; García, J.; Oseroff, S.; Cheong, S.-W. *Phys. Rev. B* **1997**, *56*, 8902.
(38) Rodríguez-Carvajal, J.; Hennion, M.; Moussa, F.; Moudden, A. H.; Pinsard, L.; Revcolevschi, A. *Phys. Rev. B* **1998**, *57*, 3189(R).
(39) Birch, F. *Phys. Rev.* **1947**, *71*, 809−824.
(40) Haumont, R.; Bouvier, P.; Pashkin, A.; Rabia, K.; Frank, S.; Dkhil, B.; Crichton, W. A.; Kuntscher, C. A.; Kreisel, J. *Phys. Rev. B* **2009**, *79*, 184110.
(41) Mizokawa, T.; Khomskii, D. I.; Sawatzky, G. A. *Phys. Rev. B* **1999**, *60*, 7309.
(42) Huang, Q.; Santoro, A.; Lynn, J. W.; Erwin, R. W.; Borchers, J. A.; Peng, J. L.; Greene, R. L. *Phys. Rev. B* **1997**, *55*, 14987.
(43) Yang, C.-H.; Koo, J.; Song, C.; Koo, T. Y.; Lee, K.-B.; Jeong, Y. H. *Phys. Rev. B* **2006**, *73*, 224112.